PLOS ONE

RESEARCH ARTICLE

Cancer stem cell-derived extracellular vesicles preferentially target MHC-II–macrophages and PD1+ T cells in the tumor microenvironment

Patricia Gonzalez-Callejo[1,2], Zihan Guo[1,3], Tahereh Ziglari[1], Natalie Marcia Claudio[1,4], Kayla Hoang Nguyen[1,3], Naoki Oshimori[1,3,4,5], Joaquim Seras-Franzoso[6], Ferdinando Pucci[1,3,4]*

1 Department of Cell, Developmental & Cancer Biology, Oregon Health and Science University, Portland, Oregon, United States of America, 2 Bionanoplasmonics Group, CIC biomaGUNE, Donostia-San Sebastián, Spain, 3 Program in Biomedical Sciences, Oregon Health and Science University, Portland, Oregon, United States of America, 4 Department of Otolaryngology-Head and Neck Surgery, Oregon Health and Science University, Portland, Oregon, United States of America, 5 Department of Dermatology, Oregon Health and Science University, Portland, Oregon, United States of America, 6 Drug Delivery and Targeting Group, Vall d'Hebron Research Institute (VHIR), Barcelona, Spain

* pucci@ohsu.edu

Abstract

Immunotherapy is an approved treatment option for head and neck squamous cell carcinoma (HNSCC). However, the response rate to immune checkpoint blockade is only 13% for recurrent HNSCC, highlighting the urgent need to better understand tumor-immune interplay, with the ultimate goal of improving patient outcomes. HNSCC present high local recurrence rates and therapy resistance that can be attributed to the presence of cancer stem cells (CSC) within tumors. CSC exhibit singular properties that enable them to avoid immune detection and eradication. How CSC communicate with immune cells and which immune cell types are preferentially found within the CSC niche are still open questions. Here, we used genetic approaches to specifically label CSC-derived extracellular vesicles (EVs) and to perform Sortase-mediated *in vivo* proximity labeling of CSC niche cells. We identified specific immune cell subsets that were selectively targeted by EV^{CSC} and that were found in the CSC niche. Native EV^{CSC} preferentially targeted MHC-II–macrophages and PD1+ T cells in the tumor microenvironment, which were the same immune cell subsets enriched within the CSC niche. These observations indicate that the use of genetic technologies able to track EVs without *in vitro* isolation are a valuable tool to unveil the biology of native EV^{CSC}.

Introduction

Head and neck squamous cell carcinoma (HNSCC) accounts for approximately 90% of oral and oropharyngeal cancer with over 400,000 new cases and more than 150,000 deaths reported

Competing interests: The authors have declared that no competing interests exist.

each year worldwide [1]. Advances in traditional treatments (surgery, radiotherapy, chemo-therapy) have failed to increase survival due to patients presenting incurable advanced-stage disease and lymph node metastasis that ultimately cause their death [2].

Immunotherapy is an approved treatment option for Head and neck squamous cell carcinoma (HNSCC) [3]. However, the response rate to immune checkpoint blockade is only 13% for recurrent HNSCC, highlighting the urgent need to better understand tumor-immune interplay, with the ultimate goal of improving patient outcomes [3].

HNSCC present high local recurrence rates and therapy resistance that can be attributed to the presence of Cancer Stem Cells (CSC) within tumors. Several cell biomarkers such as CD44 [4–6], CD133 [7, 8], SMAD Responsive Element (SRE) [9] and Aldehyde Dehydrogenase (ALDH) activity [10–13] have identified specific CSC-like populations in HNSCC tumors with enhanced tumorigenic potential and resistance to chemo- or radiotherapy. CSC exhibit unique malignant intrinsic characteristics and play key roles in tumor initiation, growth and metastasis. CSC are also believed to drive therapy resistance and tumor relapse, as they can survive and dynamically adapt to changing and unfavorable environmental conditions [14–19].

CSC exhibit singular properties that enable them to avoid immune detection and eradication [20]. Recently, a number of studies have shown that CSC contribute to the generation of an immunosuppressive, pro-tumorigenic immune milieu by regulating the activity of various immune cells in the tumor microenvironment (TME). CSC can modulate T cells, tumor-associated macrophages (TAMs) and myeloid-derived suppressor cells activity towards immuno-suppressive pathways [20–25]. Importantly, these immune cells can also sustain CSC stemness and survival [25–28]. Such complex communication network between CSC and immune cells operates through various secreted cytokines, chemokines, growth factors and proteins of the extracellular matrix (ECM) [25–29]. Whether extracellular vesicles (EVs) also play a role is still unknown.

Emerging evidence has shown that tumors can interfere with host immunity by secreting EVs [30]. EVs are defined as a heterogeneous collection of lipid bilayer membrane-enclosed vesicles naturally secreted by both prokaryotic and eukaryotic cells and that carry a complex cargo of mRNAs, lipids, metabolites, proteins and non-coding RNAs able to induce a response when signaling to EV-recipient cells [31–39]. EVs of varying size, biogenesis and cargo content can be released from a single cell. Moreover, EV secretion pattern and content can change with changes in the physiological state of the parental cell [40, 41]. Once released, EVs can interact with cells in the immediate vicinity or at distant locations via transfer through lymphatic and blood circulation. Tumor derived EVs (tEVs) can affect the proliferation, apoptosis, cytokine production and reprogramming of both innate and adaptive immune cells, thereby modifying anti-cancer immune responses [42–49]. Whether these functions belong to specific subpopulation of tEVs, such as those released by CSC, is still unclear.

Materials and methods

Cell lines and culture conditions

Parental cell lines. Murine oral squamous cell carcinoma (OSCC) cell lines MOC2 (a chemical carcinogenesis model) and mEER (a Ras-dependent, HPV16-E6/E7-dependent model) were obtained from Kerafast, Inc, and Dr. Varner (UCSD), respectively. Both cell lines were routinely maintained in IMDM/DMEM/F12 (50:25:25) supplemented with 5% fetal bovine serum (FBS), 2 mM L-Glutamine, 1x Pen/Strep solution, Hydrocortizone (25ug/uL), Cholera Toxin (0.25ug/uL), Transferrin (25ug/uL), Insulin (10ug/uL), Tri-Iodo-Thyronine (0.2ug/uL), E.G.F. (10ug/mL). All cell cultures were propagated at 37˚C and 5% CO_2 in a humidified incubator.

Lentiviral vectors.   Detailed schemes of the lentivectors employed to tag EVs are presented in S1 Fig. A brief description of the function of each LV is detailed below.

- Lentiviral (LV) transfer plasmid coding for CD63-eGFP (and *dLNGFR)* was cloned as previously described [49] and used to tag total tEVs, as EVs marker CD63-eGFP expression is subjected to the regulation of the phosphoglycerate kinase (PGK) constitutive promoter.

- LV transfer plasmids coding for ***ALDH1A1*:*CD63-eGFP*** and ***SRE*:*CD63-eGFP*** expression cassettes were designed by us and cloned by Genewiz. Those LV were used to tag CSC derived EVs as CD63-eGFP expression is subjected to the regulation of CSC specific promoters *ALDH1A1* and *SRE* [9–13].

- LV transfer plasmid coding for ***ALDH1A1*:*SrtA*** was designed by us and cloned by Genewiz. This plasmid was used to engineer CSC and their EVs to display a membrane-bound form of Sortase A (SrtA), a bacterial transpeptidase that can catalyze the transfer of reporter molecules on the surface of EV-binding cells and cells interacting with CSC.

- LV transfer plasmid coding for ***SS-mSca-LPETGG*:*mCMV-PGK*:*CD63-eGFP*** was designed by us and cloned by Genewiz. This plasmid was used to tag total tEVs and to provide SrtA substrate (mScarlet red fluorescence protein fused to the SrtA recognition sequence LPETGG). A signal sequence (SS) instructs the cell to secrete mSca in the extracellular environment.

Generation of modified cell lines expressing tEVs and tEVs^{CSC} markers.   In order to genetically label EVs, mEER and MOC2 cell lines were transduced as previously reported by our group [49]. Briefly, LV transfer plasmids were propagated in Escherichia coli DH5α. Maxiprep was performed with Endo-free Macherey-Nagel kit. Unconcentrated lentiviral vectors were generated. MOC2 and mEER cells were seeded at a concentration of 10^5 cells per well in a 6-well plate and transduced with LV vector supernatants (1:1 ratio with complete media) in the presence of 1 μg/ml polybrene (Millipore). For the simultaneous *in vivo* detection of both tEVs^{total} and tEVs^{CSC}, mEER cell line was consecutively transduced with *SS-mSca-LPETGG*:*mCMV-PGK*:*CD63-eGFP* and *ALDH1A1*:*SrtA* LV vectors in the presence of 1 μg/ml polybrene (Millipore). Engineered cell lines were cultured under the same conditions than the ones described for the parental cell lines and propagated at 37˚C and 5% CO_2 in a humidified incubator.

CSC niche cell labeling strategy.   The strategy employed to detect CSC niche cells is based on detection of surface cell-cell contacts via SrtA, which we previously developed and extensively characterized [50]. Briefly, SrtA is a membrane-bound bacterial transpeptidase, which can catalyze the transfer of a reporter on nearby cells. SrtA is engineered to be present on the outer side of membranes (**S1C and S2A Figs**). The reporter is monomeric Scarlett fluorescent protein (mSca) fused with SrtA recognition sequence (LPETGG) and with a secretory signal sequence that allows the release of mSca as an extracellular protein (**S1C Fig**). Thanks to its generic transmembrane domain, SrtA labels the cell surface as well as both CD63+ and CD81+ EVs (**S2B, S2C Fig**). When SrtA+ EVs and/or CSC come in close contact with other cells, and when the SrtA substrate mSca is present, SrtA covalently links mSca to any membrane protein with an N-terminal glycine (such as MHC-I, MHC-II, VE-Cadherin, CD19, integrins, and others) [50]. In order to control for internalization of mSca by neighbouring cells, we used a control group in which CSC do not express SrtA while the bulk of tumor cells (including CSC) still secrete mSca. The pan-tumor expression of CD63-eGFP served as internal control for total tumor-immune interactions. To establish baseline GFP fluorescence, we

used a control group lacking CD63-eGFP. The values for SrtA labelling were calculated by subtracting baseline internalization of mSca observed in the control group.

Copy number assay. Total DNA was extracted from genetically modified 200,000 mEER and MOC2 *ALDH1A1*:*CD63-eGFP* and *SRE*:*CD63-eGFP* cell lines using QIAamp DNA Micro Kit (Qiagen). LV sequence was detected using a custom taqman assay (Applied Biosystems) on RRE sequence in a Viia7 PCR system. TaqMan probes for reference genes were *ActinB*, *GusB* and *HPRT-1* (S1 Table). One copy per genome standard was used, as previously described [49].

Orosphere formation assay. Flow sorted 5000 mEER and MOC eGFP+ and eGFP- cells/ well were seeded in 6-well ultra-low attachment plates (Corner) in StemXVivo Serum-Free Tumorsphere Media (R&D Systems). Cells were cultured for 10 to 14 days, and orosphere formation efficiency was assessed manually counting the number of orospheres per well with diameters >50 μm for each condition using light microscopy.

Stem gene profile validation. Total RNA was extracted from 300,000 mEER and MOC2 (flow-sorted as *ALDH1A1*:*CD63-eGFP+/-* and *SRE*:*CD63-eGFP+/-* cells) using the RNeasy Mini Kit (Qiagen) and the RNA obtained was reverse transcribed using a HighCapacity cDNA Reverse Transcription Kit (Thermo Fisher Scientific) according to the manufacturer's instructions. The cDNA reverse transcription product was amplified with specific probes (S1 Table) by qPCR using TaqMan method (Thermo Fisher Scientific). The reaction was performed in triplicate on a Viia7 Real time PCR system (Applied Biosystems). Relative normalized quantities (NRQ) of mRNA expression were calculated using the comparative Ct method ($2^{-\Delta\Delta Ct}$) with two reference genes (GAPDH and Actin) used as endogenous controls with Excel software.

Mice and tumor challenge. Six- to eight-week-old C57BL/6J mice were purchased from Charles River Laboratories and housed under conventional conditions and provided with food and water ad libitum. Animal care was handled in accordance with the Guide for the Care and Use of Laboratory Animals of the Oregon Health & Science University (OHSU) and covered by OHSU Institutional Animal Care and Use Committee (IACUC). Euthanasia was performed in a CO_2 chamber.

For orthotopic tumor challenge, parental mEER cells (control) and genetically modified mEER *dLNGFR*:*mCMV-PGK*:*CD63-eGFP*, mEER *ALDH1A1*:*CD63-eGFP*, mEER *SRE*: *CD63-eGFP*, mEER *SS-mSca-LPETGG*:*mCMV-PGK*:*CD63-eGFP*, mEER *ALDH1A1*:*SrtA* and mEER *SS-mSca-LPETGG*:*mCMV-PGK*:*CD63-eGFP* plus *ALDH1A1*:*SrtA* cells were intradermally injected ($1x10^6$ in 50 μl of PBS) in the flank of six to eight week old C57BL/6J mice. After 12 days mice were euthanized and tumors collected, divided in two parts and processed either for flow cytometry or embedded in OCT compound for IF imaging analysis. Tumors were never allowed to grow bigger than 10mm in one dimension, as measured by caliper.

Tumors IF imaging. 5 μm thick OCT microsections from experimental tumors were mounted on glass slides for immunofluorescent labeling. Briefly, after 15' fixation with 4%PFA samples were washed in PBS-Tween 0.3% and primary antibodies, anti-rabbit eGFP (1:200, Abcam) anti-CD45 Biotin (1:200, Biolegend),anti-F4/80 Alexafluor-647 (1:200, Biolegend), anti-SOX2 (1:200 R&D) and anti-keratin 14 (1:200, Abcam) were supplemented in PBS/BSA 3% (w/v) and incubated O.N. at 4°C. Samples were further washed 3 times in PBS-Tween 0.3% before the addition of secondary antibody. Goat Anti-rabbit AlexaFluor488 1:1000 and Streptavidin AlexaFluor568 1:500 were added and incubated 1h at RT. Slides were then washed and mounted with mounting media ProLong for visualization. Tumors were imaged using a Spinning Disk Confocal microscope (Yokogawa CSU-X1 on Zeiss Axio Observer). The measurement of the distance between eGFP+ cancer cells and F480+ Macrophages was made blindly

by 3 independent observers. This distance was quantitatively assessed with ImageJ software in 5 random tumor sections per mice group. Representative images were displayed.

Flow cytometry. Tumors were mechanically dissociated into single cell suspensions as previously described [49]. Cell suspensions were stained with conjugated antibodies (Biolegend, BD or eBiosciences) and Zombie aqua (Sigma). Following strategy was used to identify cells of interest:

- Tumor cells (CD63GFP+ Zombie aqua–CD45– CD31–)

- Endothelial cells (Zombie aqua–CD45– CD31+)

- B cells (Zombie aqua–CD45+ B220+)

- Macrophages MHC-II+(Zombie aqua–CD45+ CD11b+ F4/80+ II+)

- Macrophages MHC-II- (Zombie aqua–CD45+ CD11b+ F4/80+ II-)

- Inflammatory monocytes (Zombie aqua–CD45+ CD11b+ F4/80- CD11c+)

- Resident monocytes (Zombie aqua–CD45+ CD11b+ F4/80- CD11c-)

- Neutrophils (Zombie aqua–CD45+ F4/80- CD11c- SSChii)

- Dendritic cells (Zombie aqua–CD45+ CD11c+ F4/80– II+)

- PD-1 + T cells (Zombie aqua–CD45+ F4/80- B220- CD3+ PD-1+)

- PD-1—T cells (Zombie aqua–CD45+ F4/80- B220- CD3+ PD-1-)

Fluorochromes employed were the following: eGFP, Bv421, Bv605, Bv785, PE, PerCP, PC7, APC, A700, AC7.

Single EV analysis (**S2B, S2C Fig**) was performed as previously described [50]. Briefly, a 10-fold dilution of stock EV preparations in 0.2um filtered PBS was further serially diluted 2-fold to generate a 4-point dilution series. EV dilution series was stained with the following antibodies: CD63, CD81 and Flag, all from Biolegend and diluted to 0.1 ug/ml, without washing. Control unstained EV dilution series was also prepared. For each sample, we used a SSC trigger threshold value of 200 and the window extension at 3msec. EV staining samples were performed and analyzed in triplicate. After acquisition of 60ul (out of 200ul total), Triton-X100 was added to a final concentration of 0.5% (v/v) in each well and the plate was acquired again to confirm staining of EVs.

Statistical analysis. Bar graphs display mean value ± standard error of the mean (SEM). 2-way ANOVA Holm-Sidak´s test or non-parametric Tukey´s test were employed for multiple mean comparisons. The significance threshold was established at $p < 0.05$, and significance levels were schematically assigned *$(0.01 \leq p < 0.05)$, **$(0.001 \leq p < 0.01)$, ***$(0.0001 \leq p$, ****$(0.00001 \leq p)$. All the analyses and graphs were performed using GraphPad Prism 6 software (GraphPad, San Diego).

Results

Genetic labeling of cancer stem cell-derived extracellular vesicles

Tumor secreted EVs (tEVs) represent prominent regulators of the immune response in cancer [30, 42–49]. CSC secreted EVs (tEVs^CSC) are a subset of tEVs whose immunomodulating activity is still unknown. In order to start investigating whether tEVs^CSC have a role in shaping immune cell activity in the TME, we genetically labeled tEVs^CSC with fluorescent proteins. This approach allows to avoid any bias in EV composition due to *in vitro* isolation and assumptions on *in vivo* biodistribution of tEVs [49]. In particular, we genetically engineered

murine oral squamous cell carcinoma (OSCC) cell lines to express the vesicular membrane-associated protein CD63, fused with enhanced green fluorescence protein (CD63-eGFP) under the control of a CSC-specific promoter. We tested two different CSC-specific promoters, ALDH1A1 and SRE [9–13]. As reference controls, we genetically labeled the whole population of tEVs (including tEVs^CSC) by expressing the CD63-eGFP fusion protein under a constitutive promoter (PGK). We worked on two different OSCC cell lines, a chemical carcinogenesis model (MOC2) and a Ras-dependent, HPV16-E6/E7-dependent model (mEER). MOC2 carry the same mutations observed in human HN cancers, namely Trp53, MAPK and FAT whereas mEER+ have been engineered to express Hras(G12) and HPV-E6/E7. Together, the mutational landscape of these two cell lines model >95% of human pathology. As expected, the constitutive reporter (*PGK*:*CD63-eGFP*+) showed green fluorescence in virtually all tumor cells (**Fig 1A**). On the other hand, much less CD63-eGFP+ cells were observed in both MEER and MOC2 cells carrying the vectors *ALDH1A1*:*CD63-eGFP* (**Fig 1B**; **S3A Fig**) and *SRE*:*CD63-eGFP* (**Fig 1C**, **S3B Fig**). In order to confirm that the observed differential expression of the tEVs reporter CD63-eGFP was due to the restricted expression of the *ALDH1A1* and *SRE* promoters among CSC (and not because of low transduction efficiency), a lentiviral vector (LV) copy number assay was performed. These analyses showed that mEER *SRE*:*CD63-eGFP* cells carried on average 30 LV copies per cell (CpC), and that 5 CpC were detected in mEER *ALDH1A1*:*CD63-eGFP* cells, indicating full transduction of the tumor cell populations (**Fig 1D**). Flow cytometry analysis revealed that, expectedly, positive control mEER *PGK*:*CD63-eGFP* cells showed high levels of eGFP fluorescence. eGFP fluorescence was also detected in lower levels in modified mEER *ALDH1A1*:*CD63-eGFP* and *SRE*:*CD63-eGFP* cells, suggesting that eGFP brightest cells may constitute the CSC population (**Fig 1E**). To test this hypothesis, we flow sorted the top 5% of the engineered cells based on eGFP intensity and evaluated their expression of stemness markers and ability to form orospheres in low-attachment culture. RT-qPCR assay revealed that both mEER *ALDH1A1*:*CD63-eGFP* bright and mEER *SRE*:*CD63-eGFP* bright cells showed significantly higher expression levels of the stemness markers *ALDH1A1*, *Nanog* and *SOX2* when compared to eGFP- cells (**Fig 1F**). Similarly, MOC2 *ALDH1A1*:*CD63-eGFP* bright and MOC2 *SRE*:*CD63-eGFP* bright cells showed significantly greater expression of the stemness marker *ALDH1A1* than eGFP- cells (**S3C Fig**). Importantly, flow sorted mEER *ALDH1A1*:*CD63*-eGFP bright cells efficiently formed orospheres when cultured in serum-free Low-Attachment (LA) conditions while eGFP- cells were not able to form orospheres but showed small cellular aggregations (**Fig 1G**). Similarly, MOC2 *ALDH1A1*:*CD63-eGFP* bright cells formed big cell clusters when cultured in LA conditions (**S3D Fig**). To confirm that the orospheres we obtained in culture contain *bona fide* CSC, we performed gene expression analysis on mEER *ALDH1A1*:*CD63-eGFP* bright orospheres and found that they expressed significant higher levels of the stemness markers *ALDH1A1*, *Nanog*, *Oct-4*, *CD-133 and Sox-2* than unsorted mEER *ALDH1A1*:*CD63-eGFP* cells cultured in attachment conditions (**Fig 1H**). Additionally, the *in vivo* expression of the HNSCC CSC marker SOX2 was analyzed in mice carrying tumors formed by MOC2 *SRE*:*CD63-eGFP* cells. Expectedly, only MOC2 eGFP+ cells also co- expressed SOX2 while no SOX2 expression was found in eGFP- tumor cells (**S3E Fig**). Altogether, these data confirm the ability of *ALDH1A1*:*CD63-eGFP* and *SRE*:*CD63-eGFP* expression cassettes to restrict expression of the tEV reporter within the CSC-enriched subpopulation of mEER and MOC2 cancer cell lines.

tEVs^csc preferentially target MHC-II–macrophages and PD-1+ T cells

We and others have previously investigated the interactions that occur in the TME between tEVs and immune cells [42–49]. Mononuclear phagocytes and tumor endothelial cells were
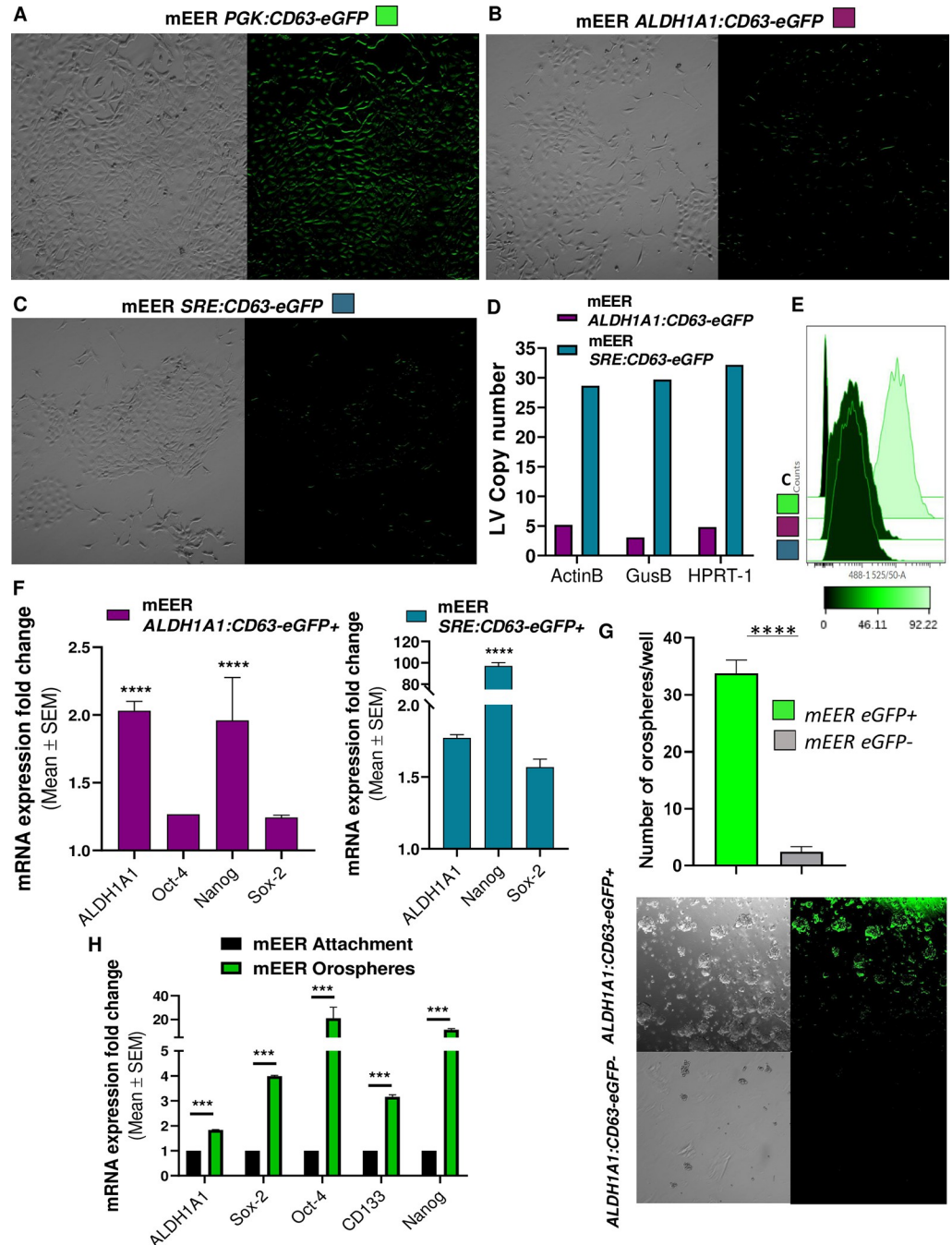
Fig 1. OSCC mEER CSC model characterization. (**A**) Representative fluorescence confocal microscopy images of in vitro cultured mEER cells stably transduced with *PGK:CD63-eGFP* reporter. Green cells represent the total tumor cells. (**B, C**) Representative fluorescence confocal microscopy images of cultured mEER cells carrying the *ALDH1A1: CD63-eGFP* or the *SRE:CD63-eGFP* expression cassettes. Green cells represent the CSC population. (**D**) Graph representing the LV copy number present in genetically modified *ALDH1A1:CD63-eGFP* and *SRE:CD63-eGFP* mEER cells assessed by PCR analysis. (**E**) Flow cytometry analysis displaying eGFP fluorescence in unmodified (Control, C) and genetically modified *PGK:CD63-eGFP* (green), *ALDH1A1:CD63-eGFP* (purple) and *SRE:CD63-eGFP* (teal) mEER cells. (**F**) Relative increase in stemness gene expression of flow sorted brightest mEER eGFP + cells compared to eGFP-cell population analyzed by RT-qPCR. (**G**) Graph depicting the number of orospheres per well generated from flow sorted brightest mEER eGFP + cells versus eGFP- cells. Representative microscopy images of orospheres growing from flow sorted *ALDH1A1:CD63-eGFP*+ mEER and *ALDH1A1:CD63-eGFP*- mEER cells cultured in 3D tumorsphere-specific medium are displayed. Green fluorescence indicates the high content of CSC in the orospheres. (**H**) RT-qPCR analysis showing the stemness gene expression signature of mEER orospheres enriched in ALDH1A1:CD63-eGFP

+ CSC compared to unmodified mEER cells growing in attachment conditions assessed by RT-qPCR. Holm-Sidak´s t test was used for statistical analysis.

among the cell types that bound tEVs at the highest rate [49]. Whether tEVs^{CSC} possess a distinct tropism toward tumor infiltrating immune cells is still unknown. In order to test if tEVs^{CSC} preferentially interact with specific immune cell subsets, we challenged mice with mEER tumor cells carrying the *ALDH1A1*:*CD63-eGFP* or the *SRE*:*CD63-eGFP* expression cassette. As control, we used mice bearing mEER tumor cells carrying the *PGK*:*CD63-eGFP* expression cassette. Flow cytometry-based analysis of tumors revealed the presence of different levels of CD63-eGFP+ cells among groups (**Fig 2A**). We then asked if differences in tEVs and tEVs^{CSC} tropism exist within functional subsets of CD45+ cells. Specifically, F4/80+ MHCII + and F4/80+ MHCII- Macrophages (Mac), inflammatory and resident monocytes (Mo), PD-1+ and PD-1- T cells, Neutrophils (Neu), B cells and dendritic cells (DC) immune subpopulations were analyzed (**S4 Fig**). In tumors formed by mEER cells constitutively expressing CD63-eGFP, CD45+ CD63-eGFP+ cells were composed mainly of MHC-II+ Mac (30.6%), B cells (16.5%) and Inflammatory Mo (16%), followed by Neu (12.9%) (**Fig 2B**). When we analyzed tumors expressing either of the tEVs^{CSC} reporters, we observed an increased fraction of CD63-eGFP+ MHC-II–Mac among CD45+ CD63-eGFP+ cells in tEVs^{CSC} reporter tumors (27.8%, average between *ALDH1A1*:*CD63-eGFP* and *SRE*:*CD63-eGFP*) compared to *PGK*: *CD63-eGFP* tumors (5.7%). Interestingly, we observed an enrichment in the interactions between mEER tEVs^{CSC} and PD-1+ T cells (11.4%), as compared to tEVs (3.4%). (**Fig 2C**). We observed statistically significant differences between the percentage of CD63-eGFP+ MHC-II + Mac infiltrating tumors constitutively expressing the tEV reporter (87.4%) and those present in tumors carrying CSC reporters (10.5%), indicating that MHC-II+ Mac predominantly uptake non-CSC tEVs. On the other hand, the percentage of CD63-eGFP+ MHC-II–Mac did not significantly change, suggesting that MHC-II–Mac predominantly uptake tEVs^{CSC} (**Fig 2D**). When we analyzed monocyte subsets, we observed a significant decrease in the percentage of CD63-eGFP+ monocytes from both inflammatory and resident subsets, indicating that monocytes predominantly uptake non-CSC tEVs. Similar results were observed with Neu, B cells and DC subsets, indicating that those populations preferably uptake non-CSC tEVs (**Fig 2D**). By labeling T cells with the activation marker PD-1, we observed that the percentage of CD63-eGFP+ PD-1+ T cells did not significantly change between tumors constitutively expressing the tEVs reporter (9.6%) and those present in tumors carrying CSC reporters (6%), suggesting that, similarly to MHC-II–Mac, also PD-1+ T cells predominantly uptake tEVs^{CSC} (**Fig 2C**). To highlight these differences, we calculated a tEVs^{CSC} specificity index by dividing the percentage of CD45+ CD63-eGFP+ immune cells for each subset in the tEVs^{CSC} groups by the percentage of the corresponding CD45+ CD63-eGFP+ subsets from the tEVs group. We observed that the index for MHC-II- Mac and PD-1+ T cells was significantly increased for those populations when compared to the index of all the other immune cell subsets. While tEVs^{CSC} specificity index mean was 0.87 for MHC-II–Mac and 0.63 for PD-1+ T cells, all other tested subsets were below 0.21 (**Fig 2E**). Altogether, these data indicate that tEVs^{CSC} possess a preferential tropism towards MHC-II–Mac and PD-1+ T cells.

Cancer stem cells and macrophages share the same niche within the tumor microenvironment

Our results so far indicate that MHC-II–Mac are selectively binding tEVs^{CSC}. We next aimed to identify the mechanisms of such preferential binding. We hypothesized that CSC and MHC-II–Mac may share the same niches within the tumor microenvironment, which would
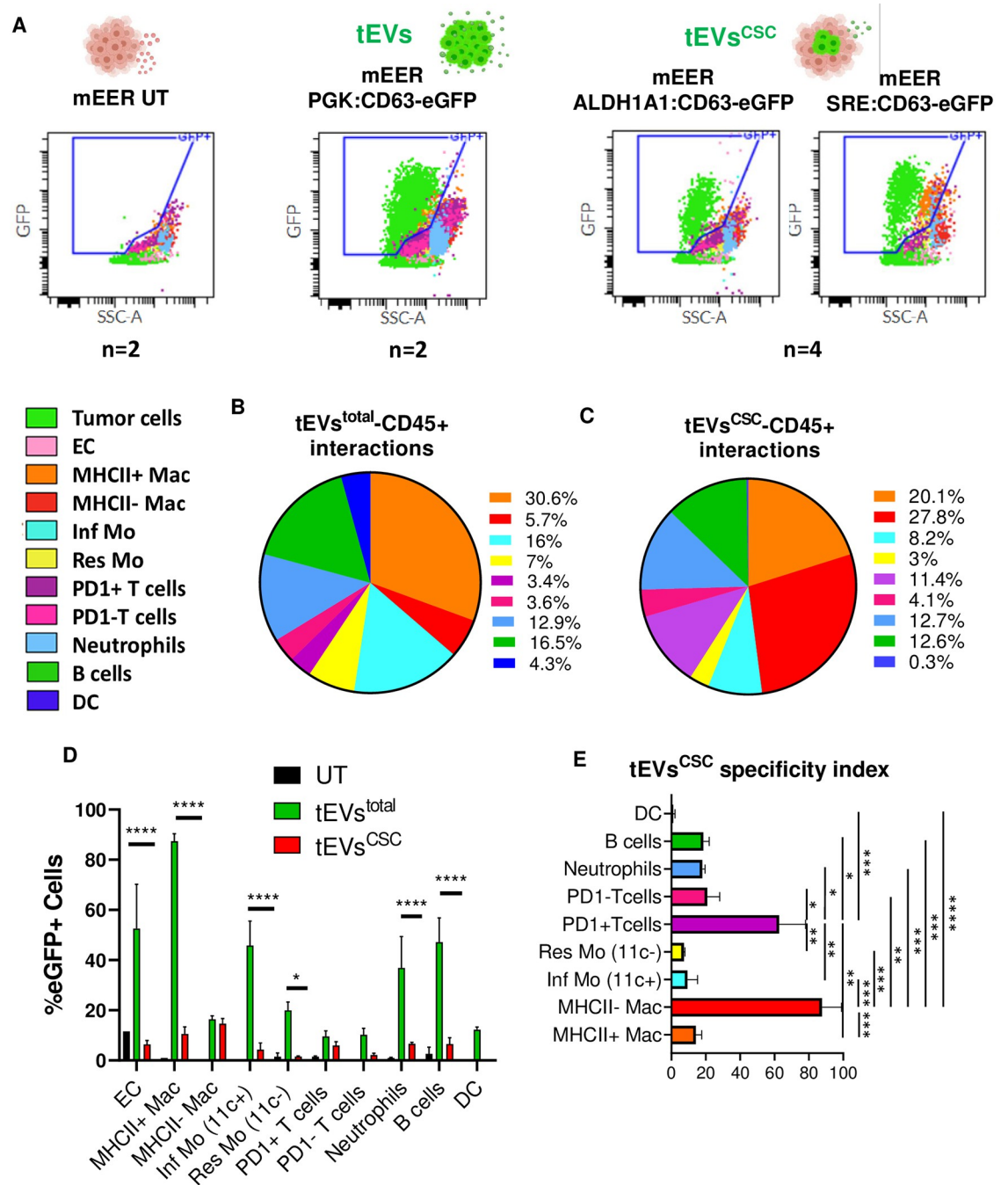
Fig 2. *In vivo* released mEER tEVs^{CSC} target MHC-II- Mac and PD-1+ T cells in the TME. (A) Representative overlaid plot of color-coded cell subsets present in tumors recovered from mice bearing genetically modified mEER cells studied by flow cytometry. Three different experimental tumor groups were analyzed: tumors formed by i) unmodified mEER cells ii) mEER cells modified with *PGK:CD63-eGFP* construct (labeling tEVs) and iii) mEER cells engineered with *ALDH1A1:CD63-eGFP* and *SRE:CD63-eGFP* LVs (labeling tEVs^{CSC}). Sample number (n) for each group is indicated below each plot. CD63-eGFP+ gate is indicated in each case. **(B)** Representative graph of the % of specific tEVs–CD45+ immune cell subsets interactions from all eGFP+ events in tumors CD45 + cells, showing a major interaction between tEVs and MHC-II+ Mac. **(C)** Representative graph of the % of specific tEVs^{CSC}–CD45 + immune cell subsets interactions from all eGFP+ events in tumors CD45+ cells, showing a major interaction between tEVs and MHC-II- Mac. **(D)** Summary graph showing the % of cell subsets presenting CD63-eGFP+ fluorescence in unlabeled EVs tumors (UT), tEV-labeled tumors and tEV^{CSC}-labeled tumors. **(E)** tEV^{CSC} specificity index showing the preferential interaction of secreted tEVs^{CSC} with specific immune cell subsets. Two-way ANOVA Tukey´s and Holm-Sidak's multiple comparisons tests were used for statistical analysis.

increase exposure to tEVs^{CSC}. We tested this hypothesis by imaging tumor sections. To this end, we performed immunofluorescence staining for CD45 and F4/80 on tumor sections from mice carrying either *PGK*:*CD63-eGFP* or *ALDH1A1*:*CD63-eGFP* expressing tumors. As expected, confocal microscopy images showed a broad CD63-eGFP+ signal in *PGK*: *CD63-eGFP* tumors (**Fig 3A**, **S5A Fig**), whereas fewer CD63-eGFP+ cells were found in *ALDH1A1*:*CD63-eGFP* tumors (**Fig 3B**, **S5B Fig**). Among CD45+ F480+ tumor macrophages, many were found at the tumor periphery. When considering those infiltrating the tumor mass, we observed a significant association of CD45+ F480+ tumor Mac with CSC, as quantified by measuring the distance between them in three distinct areas from 5 random tumor sections (**Fig 3C**). These results suggest that the location of tumor macrophages may favor their preferential uptake of tEVs^{CSC}.

Location-dependent labeling uncovers short-range interactions between CSC, tEVs^{csc} and MHC-II–Mac, PD-1+ T cells in the TME

To further investigate which immune cells are part of the CSC niche, we employed a location-dependent labeling strategy we recently validated [50]. The approach takes advantage of a membrane-bound bacterial transpeptidase, Sortase A (SrtA), which can catalyze the contact dependent transfer of a fluorescent reporter. We previously optimized and validated SrtA design, reaction requirements and efficiency *in vitro* [50]. The reporter is monomeric Scarlett fluorescent protein (mSca) fused with SrtA recognition sequence (LPETGG) and with a secretory signal sequence, which leads to the secretion of the SrtA substrate in the extracellular environment. SrtA is engineered to be present on the outer side of cellular membranes. Of note, mSca is ubiquitously expressed by all tumor cells under the control of a constitutive bi-directional promoter, along with CD63-eGFP, whereas SrtA is specifically expressed by CSC under the regulation of the *ALDH1A1* promoter (**S1C and S2A Figs**) [51]. This experimental design allows us to detect both CSC- and tEVs^{CSC}-mediated labeling of immune cells recruited to the CSC niche based on mSCA fluorescence (**Fig 4Ai**). A detailed scheme of the experimental design is presented in **Fig 4Aii**. In order to control for baseline endocytosys/phagocytosis of mSca by immune cells, we included a control group in which CSC do not express SrtA while the bulk of tumor cells (including CSC) still secrete mSca. The values for SrtA activity are calculated by subtracting this baseline internalization of mSca.

Flow cytometric analysis revealed that, as expected, the immune cell subsets most frequently interacting with tumor cells (as measured by tEV uptake) were MHC-II+ Mac (21.3% of total CD45+ CD63-GFP+ cells), followed by B cells (20.6%) and Neu (13%) (**Fig 4C**), similarly to what we observed before (**Fig 2B**). When the same tumors were analyzed to identify immune cell subsets found within the CSC niche, we found that the highest fraction of CD45+ mSca + cells corresponded to MHC-II- Mac (30.5%), followed by MHC-II+ Mac (21.4%) and PD-1 + T cells (13%) (**Fig 4D**). When we analyzed tumor-infiltrating CD45+ cell subsets presenting eGFP and mSca fluorescence, we observed a significant lower percentage of mSca+ cells compared to eGFP+ cells in all immune subsets indicating that they predominantly uptake non-CSC tEVs. Interestingly, we observed that the percentage of CD63-eGFP+ and mSca+ cells did not significantly change in MHC-II- Mac and PD-1+ T cells, suggesting that these subsets were predominantly located within the CSC niche (**Fig 4E**). We then calculated a CSC niche-specificity index to summarize these results in one value. The CSC niche-specificity index increased for MHC-II- Mac (0.63) and PD-1+ T cell subpopulation (0.44), while it remained lower than 0.23 for the rest of the immune cell subsets (**Fig 4F**). These results are consistent with a model in which MHCII- Mac and PD1+ T cells dwell in the proximity of CSC and may influence each other.
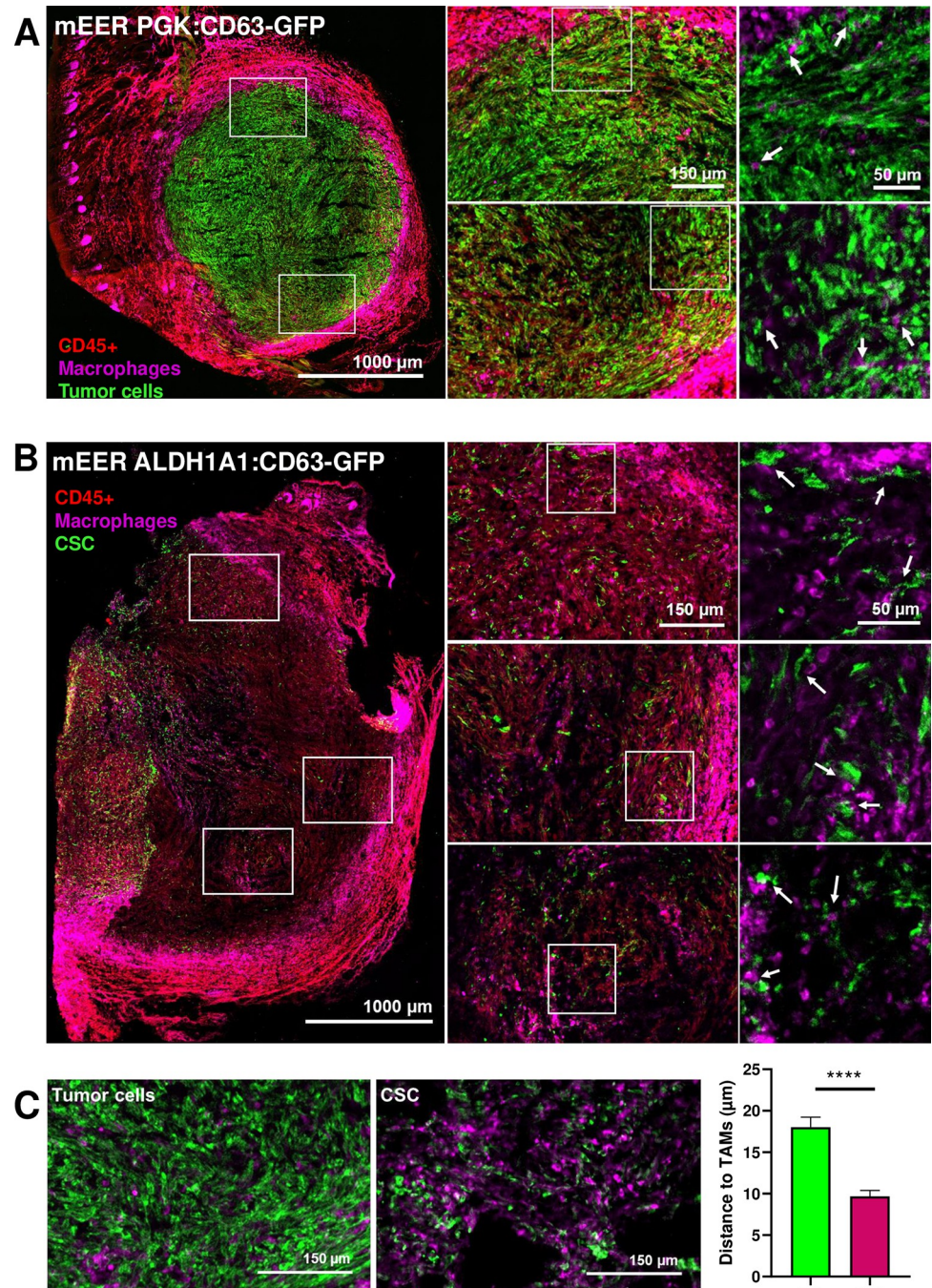
Fig 3. CSC show close localization to TAMs in the TME. (A) Representative IF images of tumor sections carrying mEER *PGK:CD63-eGFP* tumor cells. eGFP+ cells represent the total tumor cell population. Arrows in the insets indicate TAMs-tumor cells interactions. **(B)** Representative IF images of tumor sections presenting mEER *ALDH1A1: CD63-eGFP* tumor cells. eGFP+ cells represent the CSC population. Arrows in the insets indicate TAMs-CSC interactions. **(C)** Examples of analyzed tumor areas employed to measure the distance in μm observed between tumor eGFP+ cells, eGFP+ CSC and TAMs using ImageJ software. Mann-Whitney test was used for statistical analysis.
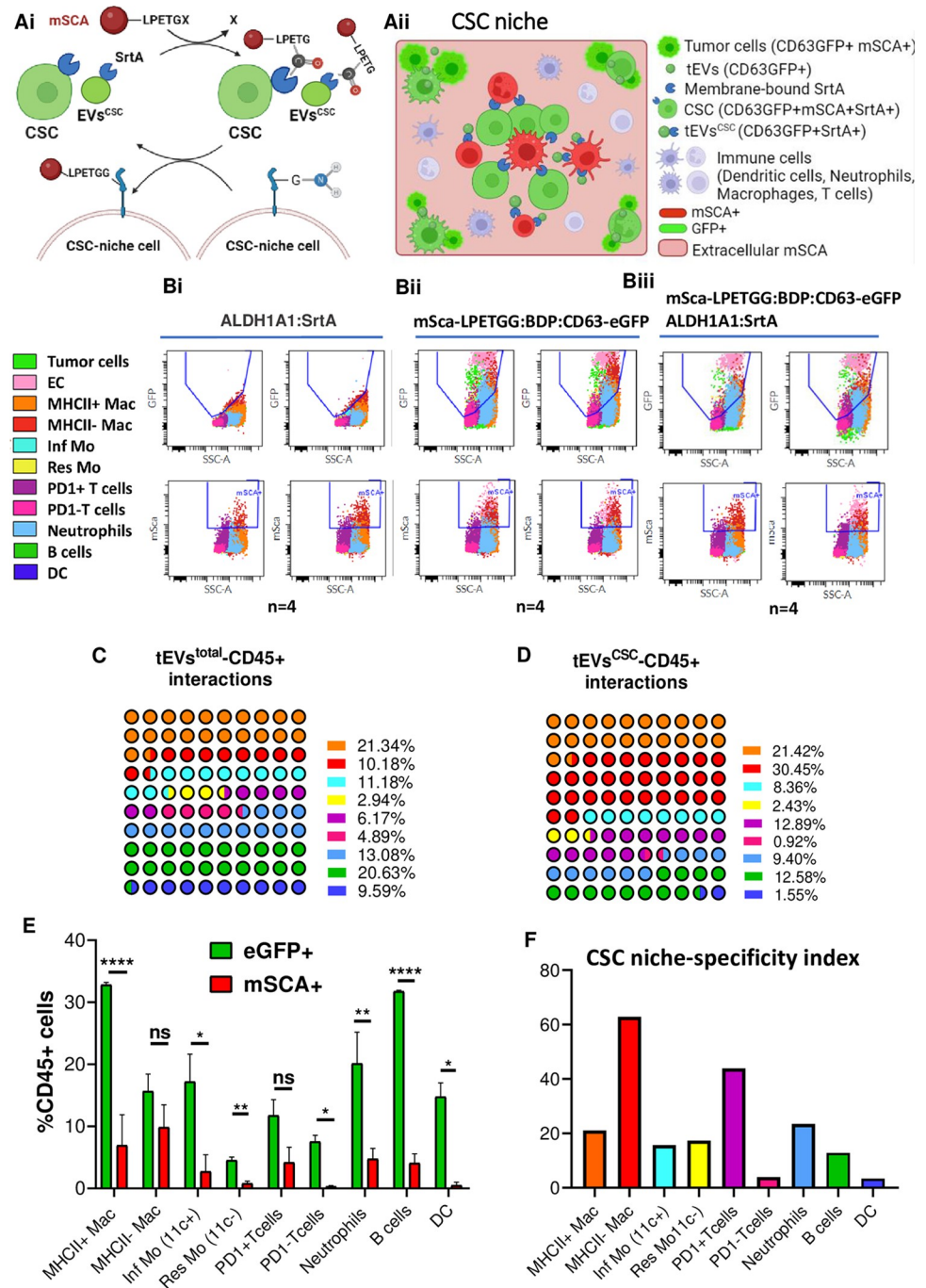
https://doi.org/10.1371/journal.pone.0279400.g003

Fig 4. Second-degree labeling via surface interactions reveals short range contacts between CSC, their tEVs^{CSC} and MHC-II–Mac, PD-1+ T cells in the CSC niche. (Ai) Illustrative schemes of SrtA enzymatic activity. SrtA present on the outer membranes of CSC and tEVs^{CSC} catalyzes the transfer of the reporter protein mSca on CSC niche cells. SrtA recognizes the sequence LPETGG. **(Aii)** Scheme summarizing experimental design to uncover the immune component in the CSC niche. Since only CSC and tEVs^{CSC} express SrtA, this strategy allows to label host cells with mSca reporter based on their proximity to CSC and their EVs. **(B)** Overlaid plot representation of different cell populations present in tumors from mice bearing genetically modified mEER cells analyzed by flow cytometry. Two plots from n = 4 are presented for each group. **(C)** Representative graphs showing the % of CD63-eGFP+ immune cells (that is, immune cells binding to tEVs) in analyzed tumors for each of the analyzed subsets with respect to all CD63-eGFP+ CD45+ immune cells. **(D)** Representative graphs showing the % of mSca+ immune cells (that is, immune cells in the proximity of CSC and their tEVs^{CSC}) for each of the analyzed subsets with respect to all mSca + CD45+ immune cells. **(E)** Summary graph presenting the % of immune cell subsets presenting CD63-eGFP+ and

mSca+ fluorescence in tumors carrying modified mEER *ALDH1A1:SrtA/mSca-LPETGG:BDP:CD63-eGFP* tumor cells test. Percentage of CD63-eGFP+ cells for each immune subset represents the % of cells that had interacted with tEVs. mSca+ cells for each immune subset represent the % of cells within the CSC niche. **(F)** CSC niche-specificity index indicating the % from tEVs^{total}-immune cell subsets interactions that correspond to specific CSC niche-immune cell subsets interactions. Two-way ANOVA Holm-Sidak´s multiple comparison test and multiple t tests were used for statistical analysis. BDP: Bi-directional promoter.

https://doi.org/10.1371/journal.pone.0279400.g004

Discussion

Tumor released EVs are key modulators of tumor immunity [30, 42–49]. The population of cancer cells is very heterogeneous, with some clones retaining stronger stem-like activity [14–19, 52, 53]. Distinguishing between the contribution of CSC from that of more differentiated cancer cells to the total tEV pool has been very challenging, especially *in vivo*. A recent study used genetic labeling of tEV-targeted cells and focused on tumor cell-to-tumor cell signaling via EVs [54]. The Authors uncovered an effective cooperation network mediated by tEVs and led by CSC, suggesting that a similar network may be in place between CSC and immune cells. Given the importance of CSC in cancer biology, new technologies that allow to dissect the influence of native tEVs^{CSC} are necessary. In this study, we present a novel strategy to effectively track CSC-derived EVs in the tumor microenvironment (TME) under physiological conditions, avoiding any *in vitro* manipulation of EVs. Here, we demonstrate proof-of-concept studies using genetic labeling of tEVs^{CSC} to identify targeted cells in the TME, with a specific focus on immune cell populations. We observed a surprising selectivity of tEVs^{CSC} in targeting specific immune cell subsets, namely MHC-II–Mac and PD-1+ T cells, which were also found enriched within the CSC niche.

Analysis of tumors with fluorescently labeled tEVs and tEVs^{CSC} showed that the fraction of immune cell subsets presenting CD63-eGFP fluorescence was higher in the tEVs labeled group than in the tEVs^{CSC} labeled group. These results are expected since tEVs^{CSC} represent a minor fraction of bulk total tEVs. Deeper analysis of CD63-eGFP+ immune cell subpopulations in tumors identified Mac as the immune cell type with the highest interaction rate with both tEVs and tEVs^{CSC}. These results are also expected, as TAMs constitute the most abundant population of tumor-infiltrating immune cells in TME [55]. TAMs are educated by environmental factors to exhibit a spectrum of polarization phenotypes usually associated with specific functional states. One key functional biomarker of TAM polarization is MHC-II [56]. Among the roles ascribed to MHC-II–Mac within the TME are immunosuppression [57, 58], lymph/angiogenesis [59], ECM deposition [60, 61] and metastasis [62]. Here, we report a clear difference between the interaction rates of MHC-II+ and MHC-II- Mac populations with each EVs fraction. While tEVs mainly interacted with MHC-II+ Mac, tEVs^{CSC} showed a significant preference toward MHC-II- Mac, as quantified by the specific interaction index. Numerous studies have shown the ability of tEVs to polarize TAMs towards pro-tumorigenic MHC-II- phenotypes [63–66]. In this respect, our data suggest that tEVs^{CSC} may be the main tEV subset responsible for the reported TAMs polarization.

Our findings provide a potential mechanistic explanation of the recently reported maintenance of CSC niche by MHC-II–Mac [26, 28, 67]. The CSC niche is particularly important to support CSC self-renewal, repopulation potential, and tumor initiation [68]. CSC contribute to the creation of a niche by inducing Mac polarization towards an immunosuppressive phenotype (MHC-II–), which in turn promotes and supports CSC aggressiveness [69–72]. The relevance of TAMs in CSC biology is reinforced by a growing list of TAM-derived factors, including IL -6, IL-8, and CXCL1, that have been implicated in the maintenance of CSC stemness in different types of cancer [69–74]. Here, we report that tEVs^{CSC} as an additional mediator targeting MHC-II–Mac. In addition, novel location-dependent labeling approaches based

on surface expression of Sortase-A demonstrated that CSC and MHC-II–Mac share the same niche. As the presence of MHC-II–Mac and CSC populations in human tumors has been correlated with a poor prognosis for many types of cancer [57, 75, 76], deeper knowledge of this communication network will be important to identify novel therapeutic opportunities.

Together with MHC-II–Mac, PD-1+ T cells also displayed specific interaction rates with tEVs^{CSC}, as compared to total tEVs. The PD-1/PD-L1 pathway is a key immunosuppressive mechanism with significant clinical implications in many solid cancer types, including HNSCC [77, 78]. Tumor EVs can also present PD-L1 on their surface, playing critical immunosuppressive roles when binding to PD-1+ T cells [79, 80]. Specifically, circulating PD-L1^{high} exosomes in HNCC patients' plasma–but not soluble PD-L1 levels, have been associated with disease progression [81]. Our study reveals that tEVs^{CSC} specifically interacted with PD-1+ T cell subsets, which may suggest the presence of PD-L1 ligand on tEVs^{CSC}. We also show that PD-1+ T cells and CSC shared the same niche. Thus, it is conceivable that tEVs^{CSC} may be primarily responsible for competing with immune checkpoint inhibitors in the clinic. For this reason, identification of the specific immune-modulators present on tEVs^{CSC} is needed to specifically target their immunosuppressive signals.

To the best of our knowledge, this work has two main limitations. First, although we are showing that generic transmembrane domains (such as that we used to tether SrtA to cell membranes) lead to labeling of EV subpopulations expressing both CD63 and CD81, we cannot exclude that other EV subsets (such as AnnexinA1+ and ARRDC1+ shedding microvesicles [82] may target different immune cells. This concern is mitigated by the fact that EV subsets are often overlapping in biomarkers [82], and by the yet unknown *in vivo* abundance of shedding microvesicles, as compared to that of multivesicular body-derived EVs. The second limitation derives from the fact that current genetic technology cannot target a reporter only to the EV compartment while avoiding expression in the parental cell which translates the reporter itself and produces the EVs.

In conclusion, the present work not only establishes a novel technological platform to study tEVs^{CSC} and their roles in the TME at the single cell level, but also identifies specific immune cell subsets linked to CSC biology. A better understanding of these microanatomical cross-talks will lead to a better knowledge of the differential effect of tEVs^{CSC} on tumor progression.

Supporting information

S1 Fig. Schematic of the lentiviral vectors (LV). (A) *dLNGFR*:*mCMV-PGK*:*CD63-eGFP* lentivector[49]. **(B)** *ALDH1A1*:*CD63-eGFP* and *SRE*:*CD63-eGFP* lentivectors. **(C)** *ALDH1A1*:*SrtA* and *SS-mSca-LPETGG*:*mCMV-PGK*:*CD63-eGFP* lentivectors.
(PDF)

S2 Fig. Flow cytometric validation of EV reporters. (A) mEER cells expressing mSca and SrtA (middle) or mSca and CD63-eGFP (right). Control untransduced cells are on the left. SrtA is detected by the Flag peptide. Note that these are constitutive expression vectors, not CSC specific. **(B-C)** Nano-flow analysis of EV preparations labeled with two fluorescent antibodies, Flag and CD63 (B) or Flag and CD81 (C). Triton treatment (top) confirms the vesicular nature of the signal.
(PDF)

S3 Fig. OSCC MOC2 CSC model. (A, B) Representative fluorescence microscopy images of cultured MOC2 *ALDH1A1*:*CD63-eGFP* cells and *SRE*:*CD63-eGFP* cells in culture. **(C)** Relative increase in stemness gene expression of flow sorted MOC2 eGFP + cells compared to eGFP-cells analyzed by RT-qPCR. **(D)** Representative images of flow sorted MOC2 *ALDH1A1*:

CD63-eGFP+ cells growing in 3D tumorspheres specific medium. (**E**) Representative IF images of tumor sections presenting MOC2 *SRE:CD63-eGFP* tumor cells. Green cells represent the CSC population. Co-expression of CSC reporters SOX2 and eGFP are found.
(PDF)

S4 Fig. Flow cytometry gating analysis of studied tumors. Example of the gating strategy used to characterize the immune cells subsets present in analyzed tumors of *in vivo* experiments using Cytobank software.
(PDF)

S5 Fig. Additional representative IF images of tumor sections carrying mEER *PGK*: *CD63-eGFP*+ (**A**) and mEER *ALDH1A1:CD63-eGFP*+ (**B**) tumor cells.
(PDF)

S1 Table. Taqman probes references (Thermo Fisher Scientific).
(DOCX)

Author Contributions

Conceptualization: Patricia Gonzalez-Callejo, Ferdinando Pucci.

Data curation: Patricia Gonzalez-Callejo.

Formal analysis: Patricia Gonzalez-Callejo.

Funding acquisition: Patricia Gonzalez-Callejo, Ferdinando Pucci.

Investigation: Patricia Gonzalez-Callejo, Zihan Guo, Tahereh Ziglari, Natalie Marcia Claudio, Kayla Hoang Nguyen.

Methodology: Patricia Gonzalez-Callejo, Joaquim Seras-Franzoso, Ferdinando Pucci.

Project administration: Ferdinando Pucci.

Resources: Naoki Oshimori, Ferdinando Pucci.

Software: Patricia Gonzalez-Callejo.

Supervision: Ferdinando Pucci.

Validation: Ferdinando Pucci.

Visualization: Patricia Gonzalez-Callejo.

Writing – original draft: Patricia Gonzalez-Callejo, Joaquim Seras-Franzoso, Ferdinando Pucci.

Writing – review & editing: Patricia Gonzalez-Callejo, Naoki Oshimori, Ferdinando Pucci.

References

1. Sung H. et al. Global Cancer Statistics 2020: GLOBOCAN Estimates of Incidence and Mortality Worldwide for 36 Cancers in 185 Countries. *CA: A Cancer Journal for Clinicians* (2021) https://doi.org/10.3322/caac.21660 PMID: 33538338

2. Johnson D. E. et al. Head and neck squamous cell carcinoma. *Nature Reviews Disease Primers* (2020) https://doi.org/10.1038/s41572-020-00224-3 PMID: 33243986

3. Moskovitz J., Moy J. & Ferris R. L. Immunotherapy for Head and Neck Squamous Cell Carcinoma. *Current Oncology Reports* vol. 20 (2018).

4. Prince M. E. et al. Identification of a subpopulation of cells with cancer stem cell properties in head and neck squamous cell carcinoma. *Proc Natl Acad Sci U S A* (2007) https://doi.org/10.1073/pnas.0610117104 PMID: 17210912

5. Roy S. et al. Inhibition of CD44 sensitizes cisplatin-resistance and affects Wnt/β-catenin signaling in HNSCC cells. *International Journal of Biological Macromolecules* (2020) https://doi.org/10.1016/j.ijbiomac.2020.01.131 PMID: 31953176

6. Gomez K. E. et al. Cancer cell CD44 mediates macrophage/ monocyte-driven regulation of head and neck cancer stem cells. *Cancer Research* (2020) https://doi.org/10.1158/0008-5472.CAN-20-1079 PMID: 32816856

7. Wei X. D. et al. In vivo investigation of CD133 as a putative marker of cancer stem cells in hep-2 cell line. *Head and Neck* (2009) https://doi.org/10.1002/hed.20935 PMID: 18853445

8. Wang J. et al. Identification and characterization of CD133+CD44+ cancer stem cells from human laryngeal squamous cell carcinoma cell lines. *J Cancer* (2017) https://doi.org/10.7150/jca.17444 PMID: 28261352

9. Oshimori N., Oristian D. & Fuchs E. TGF-β Promotes Heterogeneity and Drug Resistance in Squamous Cell Carcinoma. *Cell* 160, 963–976 (2015).

10. Chen Y. C. et al. Aldehyde dehydrogenase 1 is a putative marker for cancer stem cells in head and neck squamous cancer. *Biochemical and Biophysical Research Communications* (2009) https://doi.org/10.1016/j.bbrc.2009.05.048 PMID: 19450560

11. Chen Y. W. et al. Cucurbitacin I suppressed stem-like property and enhanced radiation-induced apoptosis in head and neck squamous carcinoma-derived CD44 +ALDH1+ cells. *Molecular Cancer Therapeutics* (2010) https://doi.org/10.1158/1535-7163.MCT-10-0504 PMID: 21062915

12. Qian X. et al. ALDH1-positive cancer stem-like cells are enriched in nodal metastases of oropharyngeal squamous cell carcinoma independent of HPV status. *Oncology Reports* (2013) https://doi.org/10.3892/or.2013.2340 PMID: 23483187

13. Clay M. R. et al. Single-marker identification of head and neck squamous cell carcinoma cancer stem cells with aldehyde dehydrogenase. *Head and Neck* (2010) https://doi.org/10.1002/hed.21315 PMID: 20073073

14. Reya T., Morrison S. J., Clarke M. F. & Weissman I. L. Stem cells, cancer, and cancer stem cells. *Nature* (2001) https://doi.org/10.1038/35102167 PMID: 11689955

15. Capp J. P. Cancer stem cells: From historical roots to a new perspective. *Journal of Oncology* vol. 2019 (2019). https://doi.org/10.1155/2019/5189232 PMID: 31308849

16. Kreso A. & Dick J. E. Evolution of the cancer stem cell model. *Cell Stem Cell* (2014) https://doi.org/10.1016/j.stem.2014.02.006 PMID: 24607403

17. Saxena K., Murali R., Kumar Jolly M. & Nair R. Cancer Stem Cell plasticity-a deadly deal. (2019) https://doi.org/10.20944/preprints201912.0388.v1

18. Gilormini M. et al. Isolation and characterization of a head and neck squamous cell carcinoma subpopulation having stem cell characteristics. *Journal of Visualized Experiments* (2016) https://doi.org/10.3791/53958 PMID: 27213496

19. Batlle E. & Clevers H. Cancer stem cells revisited. *Nature Publishing Group* 23, (2017). https://doi.org/10.1038/nm.4409 PMID: 28985214

20. Müller L. et al. Bidirectional Crosstalk Between Cancer Stem Cells and Immune Cell Subsets. *Frontiers in Immunology* (2020) https://doi.org/10.3389/fimmu.2020.00140 PMID: 32117287

21. Clara J. A., Monge C., Yang Y. & Takebe N. Targeting signalling pathways and the immune microenvironment of cancer stem cells—a clinical update. *Nature Reviews Clinical Oncology* (2020) https://doi.org/10.1038/s41571-019-0293-2 PMID: 31792354

22. Wang G. et al. Tumor microenvironment in head and neck squamous cell carcinoma: Functions and regulatory mechanisms. *Cancer Letters* (2021) https://doi.org/10.1016/j.canlet.2021.03.009 PMID: 33741424

23. Lee Y. et al. Cd44+ cells in head and neck squamous cell carcinoma suppress t-cell-mediated immunity by selective constitutive and inducible expression of PD-L1. *Clinical Cancer Research* (2016) https://doi.org/10.1158/1078-0432.CCR-15-2665 PMID: 26864211

24. Chikamatsu K., Takahashi G., Sakakura K., Ferrone S. & Masuyama K. Immunoregulatory properties of CD44+ cancer stem-like cells in squamous cell carcinoma of the head and neck. *Head and Neck* (2011) https://doi.org/10.1002/hed.21420 PMID: 20848440

25. Chen P., Hsu W. H., Han J., Xia Y. & DePinho R. A. Cancer Stemness Meets Immunity: From Mechanism to Therapy. *Cell Reports* (2021) https://doi.org/10.1016/j.celrep.2020.108597 PMID: 33406434

26. Li X. et al. CXCL12/CXCR4 pathway orchestrates CSC-like properties by CAF recruited tumor associated macrophage in OSCC. *Experimental Cell Research* (2019) https://doi.org/10.1016/j.yexcr.2019.03.013 PMID: 30857971

27. Nusblat L. M., Carroll M. J. & Roth C. M. Crosstalk between M2 macrophages and glioma stem cells. *Cellular Oncology* (2017) https://doi.org/10.1007/s13402-017-0337-5 PMID: 28643230

28. Tao W. et al. Dual Role of WISP1 in maintaining glioma stem cells and tumor-supportive macrophages in glioblastoma. *Nature Communications* (2020) https://doi.org/10.1038/s41467-020-16827-z PMID: 32541784

29. Celià-Terrassa T. & Kang Y. Metastatic niche functions and therapeutic opportunities. *Nature Cell Biology* vol. 20 868–877 (2018). https://doi.org/10.1038/s41556-018-0145-9 PMID: 30050120

30. Marar C., Starich B. & Wirtz D. Extracellular vesicles in immunomodulation and tumor progression. *Nature Immunology* (2021) https://doi.org/10.1038/s41590-021-00899-0 PMID: 33753940

31. Maas S. L. N., Breakefield X. O. & Weaver A. M. Extracellular Vesicles: Unique Intercellular Delivery Vehicles. *Trends in Cell Biology* 27, 172–188 (2017). https://doi.org/10.1016/j.tcb.2016.11.003 PMID: 27979573

32. Desrochers L. M., Antonyak M. A. & Cerione R. A. Extracellular Vesicles: Satellites of Information Transfer in Cancer and Stem Cell Biology. *Developmental Cell* (2016) https://doi.org/10.1016/j.devcel.2016.04.019 PMID: 27219060

33. Yáñez-Mó M. et al. Biological properties of extracellular vesicles and their physiological functions. *Journal of Extracellular Vesicles* (2015) https://doi.org/10.3402/jev.v4.27066 PMID: 25979354

34. Van Niel G., D'Angelo G. & Raposo G. Shedding light on the cell biology of extracellular vesicles. *Nature Reviews Molecular Cell Biology* (2018) https://doi.org/10.1038/nrm.2017.125 PMID: 29339798

35. Iraci N., Leonardi T., Gessler F., Vega B. & Pluchino S. Focus on extracellular vesicles: Physiological role and signalling properties of extracellular membrane vesicles. *International Journal of Molecular Sciences* (2016) https://doi.org/10.3390/ijms17020171 PMID: 26861302

36. György B. et al. Membrane vesicles, current state-of-the-art: Emerging role of extracellular vesicles. *Cellular and Molecular Life Sciences* (2011) https://doi.org/10.1007/s00018-011-0689-3 PMID: 21560073

37. Willms E. et al. Cells release subpopulations of exosomes with distinct molecular and biological properties. *Scientific Reports* (2016) https://doi.org/10.1038/srep22519 PMID: 26931825

38. Yoon Y. J., Kim O. Y. & Gho Y. S. Extracellular vesicles as emerging intercellular communicasomes. *BMB Reports* (2014) https://doi.org/10.5483/bmbrep.2014.47.10.164 PMID: 25104400

39. Zaborowski M. P., Balaj L., Breakefield X. O. & Lai C. P. Extracellular Vesicles: Composition, Biological Relevance, and Methods of Study. *BioScience* (2015) https://doi.org/10.1093/biosci/biv084 PMID: 26955082

40. Wen S. W. et al. Breast Cancer-Derived Exosomes Reflect the Cell-of-Origin Phenotype. *Proteomics* 19, (2019). https://doi.org/10.1002/pmic.201800180 PMID: 30672117

41. Abels E. R. & Breakefield X. O. Introduction to Extracellular Vesicles: Biogenesis, RNA Cargo Selection, Content, Release, and Uptake. *Cellular and Molecular Neurobiology* (2016) https://doi.org/10.1007/s10571-016-0366-z PMID: 27053351

42. Zhou X. et al. The function and clinical application of extracellular vesicles in innate immune regulation. *Cellular and Molecular Immunology* (2020) https://doi.org/10.1038/s41423-020-0391-1 PMID: 32203193

43. Srivastava A., Rathore S., Munshi A. & Ramesh R. Extracellular Vesicles in Oncology: from Immune Suppression to Immunotherapy. *AAPS Journal* (2021) https://doi.org/10.1208/s12248-021-00554-4 PMID: 33586060

44. Wieckowski E. U. et al. Tumor-Derived Microvesicles Promote Regulatory T Cell Expansion and Induce Apoptosis in Tumor-Reactive Activated CD8 + T Lymphocytes. *The Journal of Immunology* (2009) https://doi.org/10.4049/jimmunol.0900970 PMID: 19692638

45. Chen X. et al. Exosomes derived from hypoxic epithelial ovarian cancer cells deliver microRNAs to macrophages and elicit a tumor-promoted phenotype. *Cancer Letters* (2018) https://doi.org/10.1016/j.canlet.2018.08.001 PMID: 30098399

46. Cooks T. et al. Mutant p53 cancers reprogram macrophages to tumor supporting macrophages via exosomal miR-1246. *Nature Communications* (2018) https://doi.org/10.1038/s41467-018-03224-w PMID: 29472616

47. Mittal S., Gupta P., Chaluvally-Raghavan P. & Pradeep S. Emerging role of extracellular vesicles in immune regulation and cancer progression. *Cancers (Basel)* (2020) https://doi.org/10.3390/cancers12123563 PMID: 33260606

48. Raimondo S., Pucci M., Alessandro R. & Fontana S. Extracellular vesicles and tumor-immune escape: Biological functions and clinical perspectives. *International Journal of Molecular Sciences* 21, (2020). https://doi.org/10.3390/ijms21072286 PMID: 32225076

49. Pucci F. et al. SCS macrophages suppress melanoma by restricting tumor-derived vesicle-B cell interactions. *Science (1979)* (2016) https://doi.org/10.1126/science.aaf1328 PMID: 26989197

50. Hamilton N., Claudio N. M., Armstrong R. J. & Pucci F. Cell Surface Labeling by Engineered Extracellular Vesicles. *Advanced Biosystems* 4, (2020). https://doi.org/10.1002/adbi.202000007 PMID: 32390342

51. Amendola M., Venneri M. A., Biffi A., Vigna E. & Naldini L. Coordinate dual-gene transgenesis by lentiviral vectors carrying synthetic bidirectional promoters. *Nature Biotechnology* 23, (2005). https://doi.org/10.1038/nbt1049 PMID: 15619618

52. Phi LTH et al. Cancer Stem Cells (CSCs) in Drug Resistance and their Therapeutic Implications in Cancer Treatment. *Stem Cells Int.* (2018) https://doi.org/10.1155/2018/5416923 PMID: 29681949

53. Visvader J. E. & Lindeman G. J. Cancer stem cells: Current status and evolving complexities. *Cell Stem Cell* 10, 717–728 (2012). https://doi.org/10.1016/j.stem.2012.05.007 PMID: 22704512

54. Ruivo C. F. et al. Extracellular Vesicles from Pancreatic Cancer Stem Cells Lead an Intratumor Communication Network (EVNet) to fuel tumour progression. *Gut* gutjnl-2021-324994 (2022) https://doi.org/10.1136/gutjnl-2021-324994 PMID: 35012996

55. Baig M. S. et al. Tumor-derived exosomes in the regulation of macrophage polarization. *Inflammation Research* (2020) https://doi.org/10.1007/s00011-020-01318-0 PMID: 32162012

56. Boutilier A. J. & Elsawa S. F. Macrophage polarization states in the tumor microenvironment. *International Journal of Molecular Sciences* vol. 22 (2021). https://doi.org/10.3390/ijms22136995 PMID: 34209703

57. Noy R. & Pollard J. W. Tumor-associated macrophages: from mechanisms to therapy. *Immunity.* (2015) https://doi.org/10.1016/j.immuni.2014.06.010 PMID: 25035953

58. Colegio O. R. et al. Functional polarization of tumour-associated macrophages by tumour-derived lactic acid. *Nature* (2014) https://doi.org/10.1038/nature13490 PMID: 25043024

59. Riabov V. et al. Role of tumor associated macrophages in tumor angiogenesis and lymphangiogenesis. *Frontiers in Physiology* vol. 5 MAR (2014). https://doi.org/10.3389/fphys.2014.00075 PMID: 24634660

60. Deligne C. & Midwood K. S. Macrophages and Extracellular Matrix in Breast Cancer: Partners in Crime or Protective Allies? *Frontiers in Oncology* vol. 11 (2021). https://doi.org/10.3389/fonc.2021.620773 PMID: 33718177

61. Ahmad R. S., Eubank T. D., Lukomski S. & Boone B. A. Immune cell modulation of the extracellular matrix contributes to the pathogenesis of pancreatic cancer. *Biomolecules* vol. 11 (2021).

62. Lin Y., Xu J. & Lan H. Tumor-associated macrophages in tumor metastasis: Biological roles and clinical therapeutic applications. *Journal of Hematology and Oncology* vol. 12 (2019). https://doi.org/10.1186/s13045-019-0760-3 PMID: 31300030

63. Zhou Z. et al. CCL18 secreted from M2 macrophages promotes migration and invasion via the PI3K/Akt pathway in gallbladder cancer. *Cellular Oncology* (2019) https://doi.org/10.1007/s13402-018-0410-8 PMID: 30276551

64. Cai J., Qiao B., Gao N., Lin N. & He W. Oral squamous cell carcinoma-derived exosomes promote M2 subtype macrophage polarization mediated by exosome-enclosed miR-29a-3p. *American Journal of Physiology—Cell Physiology* (2019) https://doi.org/10.1152/ajpcell.00366.2018 PMID: 30811223

65. Li L. et al. Exosomes derived from hypoxic oral squamous cell carcinoma cells deliver miR-21 to normoxic cells to elicit a prometastatic phenotype. *Cancer Research* (2016) https://doi.org/10.1158/0008-5472.CAN-15-1625 PMID: 26992424

66. Ito A. et al. Extracellular vesicles shed from gastric cancer mediate protumor macrophage differentiation. *BMC Cancer* (2021) https://doi.org/10.1186/s12885-021-07816-6 PMID: 33509150

67. Taniguchi S. et al. Tumor-initiating cells establish an IL-33–TGF-b niche signaling loop to promote cancer progression. *Science (1979)* 369, (2020).

68. Plaks V., Kong N. & Werb Z. The cancer stem cell niche: How essential is the niche in regulating stemness of tumor cells? *Cell Stem Cell* vol. 16 225–238 (2015). https://doi.org/10.1016/j.stem.2015.02.015 PMID: 25748930

69. Kong L. et al. Deletion of interleukin-6 in monocytes/macrophages suppresses the initiation of hepatocellular carcinoma in mice. *Journal of Experimental and Clinical Cancer Research* (2016) https://doi.org/10.1186/s13046-016-0412-1 PMID: 27589954

70. Xu X., Ye J., Huang C., Yan Y. & Li J. M2 macrophage-derived IL6 mediates resistance of breast cancer cells to hedgehog inhibition. *Toxicology and Applied Pharmacology* (2019) https://doi.org/10.1016/j.taap.2018.12.013 PMID: 30578886

71. Yin Y. et al. The immune-microenvironment confers chemoresistance of colorectal cancer through macrophage-derived IL6. *Clinical Cancer Research* (2017) https://doi.org/10.1158/1078-0432.CCR-17-1283 PMID: 28928161

72. Zhu X. et al. IL-6R/STAT3/miR-204 feedback loop contributes to cisplatin resistance of epithelial ovarian cancer cells. *Oncotarget* (2017) https://doi.org/10.18632/oncotarget.16610 PMID: 28388577

73. Lu H. et al. A breast cancer stem cell niche supported by juxtacrine signalling from monocytes and macrophages. *Nature Cell Biology* (2014) https://doi.org/10.1038/ncb3041 PMID: 25266422

74. Mitchem J. B. et al. Targeting tumor-infiltrating macrophages decreases tumor-initiating cells, relieves immunosuppression, and improves chemotherapeutic responses. *Cancer Research* (2013) https://doi.org/10.1158/0008-5472.CAN-12-2731 PMID: 23221383

75. Park I. H. et al. Tumor-derived induces expression on immunosuppressive NK cells in triple-negative breast cancer. 8, 32722–32730 (2017).

76. Franklin R. A. et al. The cellular and molecular origin of tumor-associated macrophages. *Science (1979)* (2014) https://doi.org/10.1126/science.1252510 PMID: 24812208

77. Schneider S. et al. PD-1 and PD-L1 expression in HNSCC primary cancer and related lymph node metastasis–impact on clinical outcome. *Histopathology* 73, (2018).

78. Bai J. et al. Regulation of PD-1/PD-L1 pathway and resistance to PD-1/PDL1 blockade. *Oncotarget* vol. 8 (2017).

79. Poggio M. et al. Suppression of Exosomal PD-L1 Induces Systemic Anti-tumor Immunity and Memory. *Cell* (2019) https://doi.org/10.1016/j.cell.2019.02.016 PMID: 30951669

80. Chen G. et al. Exosomal PD-L1 contributes to immunosuppression and is associated with anti-PD-1 response. *Nature* (2018) https://doi.org/10.1038/s41586-018-0392-8 PMID: 30089911

81. Theodoraki M. N., Yerneni S. S., Hoffmann T. K., Gooding W. E. & Whiteside T. L. Clinical significance of PD-L1 þ exosomes in plasma of head and neck cancer patients. *Clinical Cancer Research* (2018) https://doi.org/10.1158/1078-0432.CCR-17-2664 PMID: 29233903

82. Jeppesen DK, Fenix AM, Franklin JL, et al. Reassessment of Exosome Composition. *Cell* (2019) https://doi.org/10.1016/j.cell.2019.02.029 PMID: 30951670